Mathematics

https://www.aimspress.com/journal/Math

AIMS Mathematics, 11(8): 24033–24059
DOI:10.3934/math.2026969
Received: 09 June 2026
Revised: 26 July 2026
Accepted: 31 July 2026
Published: 05 August 2026

*Research article*

# Formation mechanism of concentration and entropy-related cavitation in the pressureless limit for non-isentropic logarithmic gas dynamics

**Yiming Gao, Weifeng Jiang*** **and Chengkai Tu**

College of Science, China Jiliang University, Hangzhou 310018, China

* **Correspondence:** Email:casujiang89@gmail.com.

**Abstract:** In this paper, we study the pressureless limit of the Riemann solutions for a reduced two-phase mixtures model with non-isentropic logarithmic gas state. We construct the Riemann solutions using the $p-u$ plane projection method and study the formation of delta shock waves and vacuum as the pressure vanishes. We prove that, as pressure vanishes, the limit of Riemann solutions is the Riemann solutions of the reduced 2-dimensional pressureless gas dynamics model, where the evacuation is strictly determined by the state with higher entropic stiffness. In particular, we compare the rates at which the density of the intermediate state tends to singularity, such as infinity or vacuum, when the model is with logarithmic gas, polytropic gas, and generalized Chaplygin gas as the pressure vanishes. Then, we quantitatively demonstrated that logarithmic gases can be regarded as a transitional form between polytropic gases and generalized Chaplygin gases. Finally, numerical simulations employing essentially non-oscillatory schemes with third-order Runge-Kutta methods are used to validate the theoretical convergence behaviors.

**Keywords:** concentration and cavitation; Riemann solution; vanishing pressure; non-isentropic logarithmic gas; two-phase mixtures model
**Mathematics Subject Classification:** 35L65, 35L80, 35R35

## 1. Introduction

In this paper, we study the pressureless limit of the Riemann solutions for a reduced two-phase mixture model [1]

$$\begin{cases} \rho_t + (\rho u)_x = 0, \\ (\rho u)_t + (\rho u^2 + p(\rho, s))_x = 0, \\ (\rho s)_t + (\rho u s)_x = 0, \end{cases} \tag{1.1}$$

where $\rho, u, s$, and $p$ represent the density, velocity, specific entropy, and pressure, respectively. System (1.1) is obtained by relaxation from the two-phase mixtures model [1, 2]. It describes the dynamics of a discrete fluid volume bounded by a thin interfacial layer separating two immiscible fluids [3]. In particular, system (1.1) is extensively utilized in computational analyses of air-water two-phase flow dynamics within centrifugal pump impellers [4] and the simulation of evaporative spray systems [5]. Specifically, we focus on the non-isentropic logarithmic gas, whose equation of state (EoS) is given by

$$p = Af(s)\ln\rho, \tag{1.2}$$

where $A > 0$ is a perturbation parameter, and $f(s)$ satisfies $f'(s) > 0$. In practical physical contexts, the pure logarithmic equation of state has been widely applied in modeling various extreme physical fluids. For instance, it is used to model condensed phases under extreme compression [6], ensure causality in relativistic hydrodynamics [7], and serve as a cosmological fluid model to generate accelerating negative pressure [8–10].

The selection of the coupled form $p = Af(s)\ln\rho$ is essentially a parallel mathematical generalization. Analogous to the classical non-isentropic polytropic gases ($p = Af(s)\rho^{\gamma_1(A)}$) and the generalized Chaplygin gases ($p = -Af(s)\rho^{-\gamma_2(A)}$), we explicitly introduce the entropy function $f(s)$ into the logarithmic equation of state. The primary reason for choosing this form is to study the transition between non-isentropic polytropic gases and generalized Chaplygin gases, while theoretically investigating how "entropy differences" intervene in the formation of logarithmic gas singularities (such as vacuum states and Dirac shock waves). From a mathematical perspective, the pressure $p$ spans the entire real axis, and the unique feature of the nonlinear term $\ln\rho$ is that its singularity emerges precisely as the density tends either to infinity or to zero. Therefore, this model provides a reasonable analytical framework for studying the mechanisms of mass concentration and cavitation under non-isentropic perturbations. Furthermore, at extreme limits, the logarithmic gas exhibits asymptotic behaviors consistent with polytropic gases at high densities, and similar to generalized Chaplygin gases near vacuum states [11].

As the pressure parameter $A \to 0$, system (1.1) formally degenerates into the reduced two-dimensional pressureless gas dynamics (2-D PGD) model

$$\begin{cases} \rho_t + (\rho u)_x = 0, \\ (\rho u)_t + (\rho u^2)_x = 0, \\ (\rho s)_t + (\rho u s)_x = 0. \end{cases} \tag{1.3}$$

System (1.3) describes the collective motion of sticky particles that undergo inelastic collisions [12, 13] and elucidates cosmological structure formation through matter aggregation [14]. The formation of singular structures within this system, specifically Dirac shocks and vacuum states, has attracted considerable attention. Physically, the $\delta$-shock formation mechanism embodies the extreme concentration of particle momenta along lower-dimensional manifolds [15], while vacuum regions manifest as matter-free zones developing between interacting particle clusters [16]. The Riemann solutions for system (1.3) have been rigorously obtained by Hu et al. [17] using the vanishing viscosity method, which clearly exhibit these concentration and cavitation phenomena.

In parallel, to mathematically justify the formation of such singular structures, the vanishing pressure limit has proven to be another potent analytical tool. Pioneering works by Li [18] and

Chen and Liu [19, 20] established the concentration and cavitation mechanisms for isentropic and non-isentropic polytropic gases, demonstrating that the vanishing pressure limit of Riemann solutions to the perturbed system converges exactly to the Riemann solution of the corresponding limit system. However, while extensive vanishing pressure work has been devoted to isentropic flows, including the isentropic two-phase logarithmic model [21, 22], logarithmic traffic flow models [23], relativistic logarithmic dynamics [24], the pressureless Euler equations modeling acoustic generation [25], the Umami Chaplygin Aw-Rascle model [26], and other compressible fluids [27–29], the fundamentally distinct mechanisms within non-isentropic singular limits remain relatively unexplored.

In this study, we are concerned with the Riemann problem for systems (1.1) and (1.2) subject to the initial data

$$(\rho, u, s)|_{t=0} = \begin{cases} (\rho_l, u_l, s_l), & x < 0, \\ (\rho_r, u_r, s_r), & x > 0, \end{cases} \tag{1.4}$$

where $\rho_{l,r} > 0$, $u_{l,r}$, and $s_{l,r}$ are given constants.

Solving this Riemann problem and analyzing the limiting behavior for the non-isentropic logarithmic gas presents mathematical difficulties. Specifically, the classical $\rho - u$ plane projection method [30] fails because the wave curves depend explicitly on the specific entropy. Consequently, curves corresponding to different entropy states intersect and overlap in the two-dimensional phase plane [19, 31]. Furthermore, the non-isentropic coupling introduces additional intermediate states, making the explicit formulation of implicit functions challenging. To overcome these hurdles, we analyze the problem in the three-dimensional $(p, u, s)$ phase space. By determining the monotonicity and convexity of the elementary wave curves, this spatial approach clearly partitions the phase space, enabling the direct construction of exact Riemann solutions. Therefore, the primary purpose of this paper is to construct the exact Riemann solutions for systems (1.1) and (1.2), calculate their vanishing pressure limits as $A \to 0$, and conduct precise asymptotic comparisons against polytropic [19, 32] and generalized Chaplygin gases [33–36] to quantify the convergence speeds of these singular forms.

Our main findings are as follows. As $A \to 0$, we reveal distinct singular phenomena driven by the logarithmic nonlinearity. For $u_l > u_r$, an exponential mass concentration ($\rho \sim e^{C/A}$) triggers the formation of $\delta$-shocks. This extreme accumulation overpowers the algebraic growth of polytropic gases, dictating a principal scaling transition $\gamma(A) = \mathcal{O}(A \ln(1/A))$. Conversely, for $u_l < u_r$, an asymmetric vacuum emerges governed by entropic stiffness, which fundamentally contrasts the symmetric evacuation of generalized Chaplygin gases [33, 34]. Matching their macroscopic decay scales necessitates a continuous piecewise equivalent index. Ultimately, these results highlight the inherent structural instability and extreme singular mechanisms of the logarithmic equation of state.

Finally, we employ essentially non-oscillatory (ENO) schemes coupled with third-order Runge-Kutta methods [37] to visually validate the theoretical convergence behaviors, demonstrating strict alignment with our analytical predictions.

The structure of this paper is outlined below. In Section 2, we briefly review the Riemann solutions to the 2-D PGD model (1.3). In Section 3, we construct the Riemann solutions of the non-isentropic logarithmic gas systems directly in the 3D phase space. In Sections 4 and 5, we investigate the vanishing pressure limits and clarify the formation mechanisms of $\delta$-shocks and vacuum states. In Section 6, we perform asymptotic comparisons to reveal the convergence speeds of the singularities. Finally, in Section 7, numerical experiments are presented to confirm the validity of our theory.

## 2. Riemann solutions for the Reduced 2-D PGD model (1.3)

In this section, we briefly review the Riemann solutions for the reduced 2-D PGD model (1.3) with the initial Riemann data (1.4). More details can be found in [38].

The reduced 2-D PGD model (1.3) possesses a triple eigenvalue $\lambda = u$ and two corresponding right eigenvectors $\vec{r}_1 = (1,0,0)^T$ and $\vec{r}_2 = (0,0,1)^T$. Since $\nabla\lambda \cdot \vec{r}_i \equiv 0\,(i = 1,2)$, system (1.3) is linearly degenerate. Based on the characteristic analysis and the generalized Rankine-Hugoniot conditions, the Riemann solutions for (1.3) and (1.4) can be constructed by the following three cases.

When $u_l < u_r$, the Riemann solution consists of two contact discontinuities bounding a vacuum state. The solution can be expressed as

$$(\rho, u, s)(\xi) = \begin{cases} (\rho_l, u_l, s_l), & \xi < u_l, \\ (0, u(\xi), s(\xi)), & u_l < \xi < u_r, \\ (\rho_r, u_r, s_r), & \xi > u_r, \end{cases} \tag{2.1}$$

where $\xi = x/t$, and the vacuum region forms between the characteristics $\xi = u_l$ and $\xi = u_r$.

When $u_l = u_r$, the Riemann solution consists of a single contact discontinuity separating two constant states. The solution is given by

$$(\rho, u, s)(\xi) = \begin{cases} (\rho_l, u_l, s_l), & \xi < u_l, \\ (\rho_r, u_r, s_r), & \xi > u_l. \end{cases} \tag{2.2}$$

In this case, the contact discontinuity propagates with speed $u = u_l = u_r$.

When $u_l > u_r$, the characteristics overlap, and the left state $(\rho_l, u_l, s_l)$ is connected to the right state $(\rho_r, u_r, s_r)$ by a $\delta$-shock wave. Let $S = \{(x(t), t) : t \geq 0\}$ be the trajectory of the discontinuity. A two-dimensional weighted delta function $w(t)\delta_S$ supported on $S$ is defined by

$$\langle w(t)\delta_S, \phi(x,t)\rangle = \int_0^{+\infty} w(t)\phi(x(t), t)dt, \tag{2.3}$$

for any test function $\phi(x,t) \in C_0^\infty(\mathbb{R} \times \mathbb{R}^+)$. The Riemann solution involving a $\delta$-shock wave can be expressed as

$$(\rho, u, s)(x,t) = \begin{cases} (\rho_l, u_l, s_l), & x < u_\delta t, \\ (w(t)\delta(x - u_\delta t), u_\delta, s_\delta), & x = u_\delta t, \\ (\rho_r, u_r, s_r), & x > u_\delta t, \end{cases} \tag{2.4}$$

where $u_\delta$, $s_\delta$, and $w(t)$ represent the velocity, specific entropy, and weight of the $\delta$-shock wave, respectively. To determine these quantities, we apply the generalized Rankine-Hugoniot conditions for the system of conservation laws

$$\begin{cases} \dfrac{dx(t)}{dt} = u_\delta, \\ \dfrac{dw(t)}{dt} = u_\delta[\rho] - [\rho u], \\ \dfrac{d(w(t)u_\delta)}{dt} = u_\delta[\rho u] - [\rho u^2], \\ \dfrac{d(w(t)s_\delta)}{dt} = u_\delta[\rho s] - [\rho u s], \end{cases} \tag{2.5}$$

supplemented with the entropy condition $u_r < u_\delta < u_l$. Here, $[F] = F_r - F_l$ denotes the jump of the physical quantity $F$ across the discontinuity. Solving the system of ordinary differential equations (2.5) with initial data $x(0) = 0, w(0) = 0$, we obtain

$$u_\delta = \frac{\sqrt{\rho_l}u_l + \sqrt{\rho_r}u_r}{\sqrt{\rho_l} + \sqrt{\rho_r}}, \quad s_\delta = \frac{\sqrt{\rho_l}s_l + \sqrt{\rho_r}s_r}{\sqrt{\rho_l} + \sqrt{\rho_r}}, \quad w(t) = \sqrt{\rho_l\rho_r}(u_l - u_r)t. \tag{2.6}$$

This solution indicates that the mass, momentum, and total entropy concentrate on the shock front, forming a Dirac measure. In addition, we prove that (2.4) satisfies the weak formulation in the sense of distributions

$$\langle \rho, \phi_t \rangle + \langle \rho u, \phi_x \rangle = 0, \quad \langle \rho u, \phi_t \rangle + \langle \rho u^2, \phi_x \rangle = 0, \quad \langle \rho s, \phi_t \rangle + \langle \rho u s, \phi_x \rangle = 0, \tag{2.7}$$

for arbitrary $\phi \in C_0^{+\infty}(\mathbb{R} \times \mathbb{R}^+)$, in which the integral terms are defined as

$$\langle \rho, \phi \rangle = \int_0^{+\infty} \int_{-\infty}^{+\infty} \rho_0(x,t)\phi(x,t)\,dxdt + \langle w_1(t)\delta_S, \phi(u_\delta t, t) \rangle, \tag{2.8}$$

and $\langle \rho u, \phi \rangle, \langle \rho s, \phi \rangle$ have definitions similar to $\rho_0 u_0, \rho_0 s_0, w_2(t)$, and $w_3(t)$ in integral form as above, where

$$\begin{cases} w_1(t) = t(u_\delta[\rho] - [\rho u]), & \rho_0 = \rho_l + [\rho]H(x - u_\delta t), \\ w_2(t) = t(u_\delta[\rho u] - [\rho u^2]), & u_0 = u_l + [u]H(x - u_\delta t), \\ w_3(t) = t(u_\delta[\rho s] - [\rho u s]), & s_0 = s_l + [s]H(x - u_\delta t). \end{cases} \tag{2.9}$$

Here, $H(x)$ is the Heaviside function given by

$$H(x) = \begin{cases} 1, & x > 0, \\ 0, & x < 0. \end{cases} \tag{2.10}$$

## 3. The Riemann solutions for the non-isentropic generalized logarithmic gas state

### 3.1. Preliminaries

In this section, we introduce the basic quantities and properties for systems (1) and (2). The eigenvalues for (1) and (2) are

$$\lambda_1^A = u - \sqrt{\frac{Af(s)}{\rho}} < \lambda_2^A = u < \lambda_3^A = u + \sqrt{\frac{Af(s)}{\rho}}, \tag{3.1}$$

and the corresponding right eigenvectors are

$$r_1^A = \left(-\rho, \sqrt{\frac{Af(s)}{\rho}}, 0\right)^T, \quad r_2^A = (\rho f'(s)\ln\rho, 0, -f(s))^T, \quad r_3^A = \left(\rho, \sqrt{\frac{Af(s)}{\rho}}, 0\right)^T, \tag{3.2}$$

respectively. In terms of $\nabla = \left(\partial_\rho, \partial_u, \partial_s\right)$, calculating $\nabla\lambda_i \cdot r_i$, we find that

$$\nabla\lambda_1^A \cdot r_1^A = -\frac{1}{2}\sqrt{\frac{Af(s)}{\rho}} < 0, \quad \nabla\lambda_2^A \cdot r_2^A \equiv 0, \quad \nabla\lambda_3^A \cdot r_3^A = \frac{1}{2}\sqrt{\frac{Af(s)}{\rho}} > 0, \tag{3.3}$$

which shows that $\lambda_1^A$ and $\lambda_3^A$ are genuinely nonlinear while $\lambda_2^A$ is linearly degenerate. In addition, the Riemann invariants corresponding to three eigenvalues are

$$z_1 = \left\{ s, u - 2\sqrt{\frac{Af(s)}{\rho}} \right\}, \quad z_2 = \{u, p\}, \quad z_3 = \left\{ s, u + 2\sqrt{\frac{Af(s)}{\rho}} \right\}, \tag{3.4}$$

respectively.

### 3.2. *The classical waves for* (1.1) *and* (1.2)

In this section, we shall discuss the Riemann solutions consisting of classical waves. From Subsection 3.1, the classical waves of (1.1) and (1.2) contain three families of elementary waves. The first and third families consist of rarefaction and shock waves, while the second family is a contact discontinuity. For convenience, we denote the $i$th rarefaction wave, the $i$th shock wave, and the contact discontinuity as $R_i$, $S_i$, and $J_2$, respectively, for $i = 1, 3$.

According to the self-similar characteristic analysis, the 1-rarefaction wave $R_1$ centered at $(\rho_l, u_l, s_l)$ is expressed as

$$R_1(\rho_l, u_l, s_l) : \begin{cases} \xi = u - \sqrt{\frac{Af(s)}{\rho}}, \\ u - 2\sqrt{\frac{Af(s)}{\rho}} = u_l - 2\sqrt{\frac{Af(s_l)}{\rho_l}}, \\ s = s_l, \quad \rho < \rho_l, \end{cases} \tag{3.5}$$

where $\xi = x/t$. Similarly, the 3-rarefaction wave $R_3$ centered at $(\rho_l, u_l, s_l)$ is given by

$$R_3(\rho_l, u_l, s_l) : \begin{cases} \xi = u + \sqrt{\frac{Af(s)}{\rho}}, \\ u + 2\sqrt{\frac{Af(s)}{\rho}} = u_l + 2\sqrt{\frac{Af(s_l)}{\rho_l}}, \\ s = s_l, \quad \rho > \rho_l. \end{cases} \tag{3.6}$$

Since the contact discontinuity is the limiting case of wave interactions, we characterize the contact discontinuity $J_2$ centered at $(\rho_l, u_l, s_l)$ as

$$J_2(\rho_l, u_l, s_l) : \begin{cases} \xi = u = u_l, \\ p = p_l \implies Af(s)\ln\rho = Af(s_l)\ln\rho_l, \end{cases} \tag{3.7}$$

based on the linear degeneracy of the second characteristic field.

Next, we consider the shock waves. The Rankine-Hugoniot conditions for system (1.1) are

$$\sigma[\rho] = [\rho u], \quad \sigma[\rho u] = [\rho u^2 + p], \quad \sigma[\rho s] = [\rho u s], \tag{3.8}$$

where $\sigma$ denotes the shock speed and $[W] = W - W_l$ denotes the jump of the quantity $W$ across the discontinuity.

If $\sigma = u$, we obtain $p = p_l$ and $u = u_l$, which implies that the contact discontinuity is a special type of discontinuity satisfying the Rankine-Hugoniot conditions.

If $\sigma \neq u$, by eliminating $\sigma$ and simplifying (3.8), we deduce

$$\begin{cases} [u] = \pm\sqrt{-Af(s)[\ln\rho][\rho^{-1}]}, \\ [s] = 0. \end{cases} \tag{3.9}$$

Considering the Lax entropy condition for the 1-shock wave

$$\lambda_1(\rho, u, s) < \sigma < \lambda_1(\rho_l, u_l, s_l), \quad \sigma < \lambda_2(\rho, u, s), \tag{3.10}$$

we can derive the expressions for $S_1(\rho_l, u_l, s_l)$ as

$$S_1(\rho_l, u_l, s_l) : \begin{cases} \sigma_1 = u_l - \sqrt{\frac{\rho Af(s)(\ln\rho - \ln\rho_l)}{\rho_l(\rho-\rho_l)}}, \\ u = u_l - \sqrt{Af(s)(\ln\rho - \ln\rho_l)\left(\frac{1}{\rho_l} - \frac{1}{\rho}\right)}, \\ s = s_l, \quad \rho > \rho_l. \end{cases} \tag{3.11}$$

Analogously, the expressions for $S_3(\rho_l, u_l, s_l)$ are

$$S_3(\rho_l, u_l, s_l) : \begin{cases} \sigma_3 = u_l + \sqrt{\frac{\rho Af(s)(\ln\rho - \ln\rho_l)}{\rho_l(\rho-\rho_l)}}, \\ u = u_l + \sqrt{Af(s)(\ln\rho - \ln\rho_l)\left(\frac{1}{\rho_l} - \frac{1}{\rho}\right)}, \\ s = s_l, \quad \rho < \rho_l. \end{cases} \tag{3.12}$$

From (3.11) and (3.12), it is evident that for systems (1) and (2), the entropy $s$ remains constant along the shock curves, which distinguishes this model from the classical non-isentropic Euler equations.

### *3.3. The Riemann solutions consisting of classical waves for (1) and (2)*

In this section, we construct the Riemann solutions consisting of classical waves. Based on the analysis in Subsection 3.2, $p$ and $u$ are Riemann invariants along the second family waves, while $s$ is the Riemann invariant along both the first and third family waves. Consequently, it is appropriate to construct the solutions in the $(p, u, s)$ phase space.

By rewriting the classical wave curves (3.5)-(3.12) in terms of the $(p, u, s)$ coordinates, the expressions for the 1-rarefaction wave $R_1$ and 1-shock wave $S_1$ centered at $(p_l, u_l, s_l)$ become

$$R_1(p_l, u_l, s_l) : \begin{cases} u - u_l = 2\sqrt{Af(s_l)}\left(e^{-\frac{p}{2Af(s_l)}} - e^{-\frac{p_l}{2Af(s_l)}}\right), \\ s = s_l, \quad p < p_l, \end{cases} \tag{3.13}$$

and

$$S_1(p_l, u_l, s_l) : \begin{cases} u - u_l = -\sqrt{(p - p_l)\left(e^{-\frac{p_l}{Af(s_l)}} - e^{-\frac{p}{Af(s_l)}}\right)}, \\ s = s_l, \quad p > p_l, \end{cases} \tag{3.14}$$

respectively. Analogously, the expressions for $R_3$ and $S_3$ centered at $(p_l, u_l, s_l)$ are given by

$$R_3(p_l, u_l, s_l) : \begin{cases} u - u_l = -2\sqrt{Af(s_l)}\left(e^{-\frac{p}{2Af(s_l)}} - e^{-\frac{p_l}{2Af(s_l)}}\right), \\ s = s_l, \quad p > p_l, \end{cases} \tag{3.15}$$

and

$$S_3(p_l, u_l, s_l) : \begin{cases} u - u_l = -\sqrt{(p - p_l)\left(e^{-\frac{p_l}{Af(s_l)}} - e^{-\frac{p}{Af(s_l)}}\right)}, \\ s = s_l, \quad p < p_l. \end{cases} \tag{3.16}$$

From (3.13) and (3.14), we verify the geometric properties of the wave curves

$$\frac{\partial u}{\partial p} = -\frac{1}{\sqrt{Af(s_l)}} e^{-\frac{p}{2Af(s_l)}} < 0, \quad \frac{\partial^2 u}{\partial p^2} = \frac{1}{2(Af(s_l))^{3/2}} e^{-\frac{p}{2Af(s_l)}} > 0 \tag{3.17}$$

for $R_1(p_l, u_l, s_l)$, and

$$\frac{u - u_l}{p - p_l} = -\sqrt{\frac{1}{p - p_l}\left(e^{-\frac{p_l}{Af(s_l)}} - e^{-\frac{p}{Af(s_l)}}\right)} < 0, \quad \left(\frac{u - u_l}{p - p_l}\right)_p > 0 \tag{3.18}$$

for $S_1(p_l, u_l, s_l)$. This geometric property rigorously indicates that the first-family rarefaction and shock wave curves are strictly decreasing and convex in the $s = s_l$ plane. Analogously, based on (3.15) and (3.16), the third-family wave curves are verified to be strictly increasing and concave in the $s = s_l$ plane.

Furthermore, to ensure a well-defined global wave structure, we establish the following asymptotic limits for the elementary wave curves centered at $(p_l, u_l, s_l)$ under extreme pressure regimes

$$\lim_{p \to -\infty} u = +\infty \quad \text{for} \quad R_1(p_l, u_l, s_l), \qquad \lim_{p \to +\infty} u = -\infty \quad \text{for} \quad S_1(p_l, u_l, s_l),$$

$$\lim_{p \to -\infty} u = -\infty \quad \text{for} \quad S_3(p_l, u_l, s_l), \qquad \lim_{p \to +\infty} u = u_l + 2\sqrt{\frac{Af(s_l)}{\rho_l}} \quad \text{for} \quad R_3(p_l, u_l, s_l).$$

These distinct asymptotic behaviors, ranging from infinite divergence to a uniquely bounded limit, guarantee a complete and rigorous topological partition of the $(p, u, s)$ phase space. Crucially, the bounded limit of the 3-rarefaction wave mathematically foreshadows the onset of cavitation dynamics under intense rarefaction conditions.

For system (1.1) with an isentropic gas state, the $p - u$ plane projection method is a standard technique for constructing Riemann solutions. However, for the non-isentropic generalized logarithmic gas, this method is inapplicable. Consider two points $A(p_l, u_l, s_l)$ and $B(p_l, u_l, s_L)$ in the phase space with $s_L > s_l$. The projections of the 1-rarefaction waves $R_1(A)$ and $R_1(B)$ onto the $p - u$ plane are

$$u = u_l + 2\sqrt{Af(s_l)}\left(e^{-\frac{p}{2Af(s_l)}} - e^{-\frac{p_l}{2Af(s_l)}}\right), \quad p < p_l, \tag{3.19}$$

and

$$u = u_l + 2\sqrt{Af(s_L)}\left(e^{-\frac{p}{2Af(s_L)}} - e^{-\frac{p_l}{2Af(s_L)}}\right), \quad p < p_l. \tag{3.20}$$

Since $f'(s) > 0$, we have $u(p, s_L) \neq u(p, s_l)$, demonstrating that the wave curves depend explicitly on entropy. Consequently, the classical projection method fails, leading us to partition the solvable domain directly in the $(p, u, s)$ coordinate system.

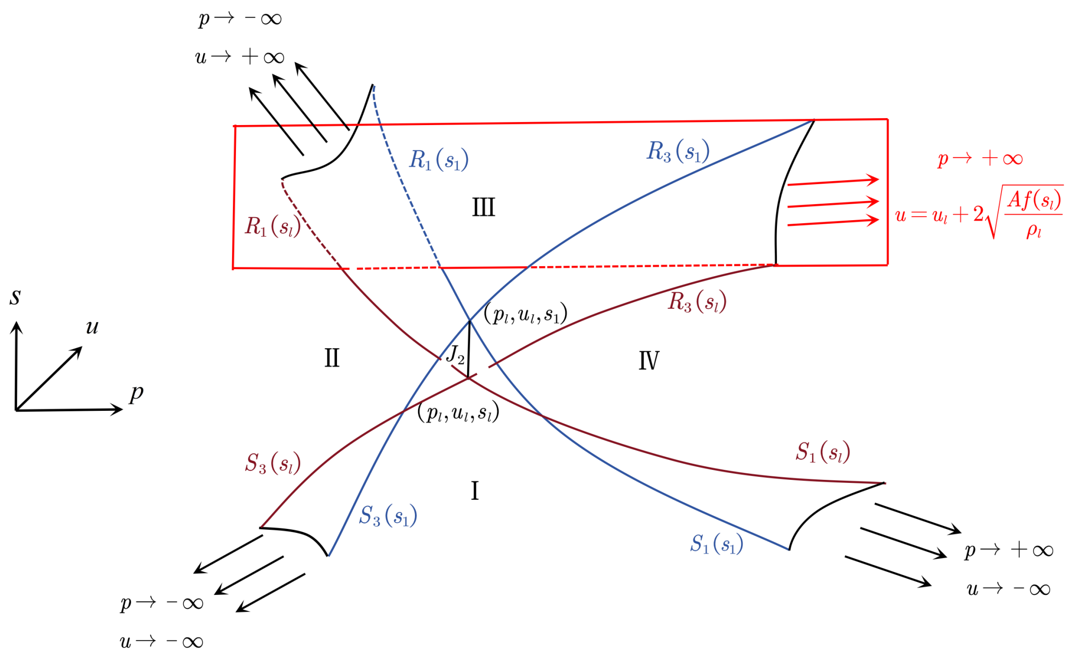


**Figure 1.** Classification of Riemann solution types for (1.1), (1.2), and (1.4).

We divide the $p-u-s$ phase space $\Omega = \{(p,u,s) : p \in \mathbb{R}, u \in \mathbb{R}, s \in \mathbb{R}\}$ into four distinct regions I, II, III, and IV (see Figure 1). These regions are partitioned by two-dimensional elementary wave surfaces, which are formed by a family of curves generated from the center $(p_l, u_l, s_l)$. These surfaces are strictly defined by the inequality conditions on pressure $p$ and velocity $u$ given in (3.13)-(3.16). The Riemann solutions for (1.1), (1.2), and (1.4) are constructed as follows:

(1) When $(p_r, u_r, s_r) \in I$, the solution consists of a 1-shock, a contact discontinuity, and a 3-shock:

$$(p_l, u_l, s_l) \xrightarrow{S_1} (p_1, u_1, s_l) \xrightarrow{J_2} (p_1, u_1, s_r) \xrightarrow{S_3} (p_r, u_r, s_r), \tag{3.21}$$

where the intermediate state $(p_1, u_1)$ is determined by

$$\begin{cases} u_1 - u_l = -\sqrt{(p_1 - p_l)\left(e^{-\frac{p_l}{Af(s_l)}} - e^{-\frac{p_1}{Af(s_l)}}\right)}, \\ u_r - u_1 = -\sqrt{(p_1 - p_r)\left(e^{-\frac{p_r}{Af(s_r)}} - e^{-\frac{p_1}{Af(s_r)}}\right)}. \end{cases} \tag{3.22}$$

(2) When $(p_r, u_r, s_r) \in II$, the solution involves a 1-rarefaction wave, a contact discontinuity, and a 3-shock:

$$(p_l, u_l, s_l) \xrightarrow{R_1} (p_1, u_1, s_l) \xrightarrow{J_2} (p_1, u_1, s_r) \xrightarrow{S_3} (p_r, u_r, s_r), \tag{3.23}$$

where $(p_1, u_1)$ satisfies

$$\begin{cases} u_1 - u_l = 2\sqrt{Af(s_l)}\left(e^{-\frac{p_1}{2Af(s_l)}} - e^{-\frac{p_l}{2Af(s_l)}}\right), \\ u_r - u_1 = -\sqrt{(p_1 - p_r)\left(e^{-\frac{p_r}{Af(s_r)}} - e^{-\frac{p_1}{Af(s_r)}}\right)}. \end{cases} \tag{3.24}$$

(3) When $(p_r, u_r, s_r) \in III$, the solution consists of two rarefaction waves separated by a contact discontinuity:

$$(p_l, u_l, s_l) \xrightarrow{R_1} (p_1, u_1, s_l) \xrightarrow{J_2} (p_1, u_1, s_r) \xrightarrow{R_3} (p_r, u_r, s_r), \tag{3.25}$$

where $(p_1, u_1)$ satisfies

$$\begin{cases} u_1 - u_l = 2\sqrt{Af(s_l)}\left(e^{-\frac{p_1}{2Af(s_l)}} - e^{-\frac{p_l}{2Af(s_l)}}\right), \\ u_r - u_1 = 2\sqrt{Af(s_r)}\left(e^{-\frac{p_1}{2Af(s_r)}} - e^{-\frac{p_r}{2Af(s_r)}}\right). \end{cases} \tag{3.26}$$

(4) When $(p_r, u_r, s_r) \in IV$, the solution involves a 1-shock, a contact discontinuity, and a 3-rarefaction wave:

$$(p_l, u_l, s_l) \xrightarrow{S_1} (p_1, u_1, s_l) \xrightarrow{J_2} (p_1, u_1, s_r) \xrightarrow{R_3} (p_r, u_r, s_r), \tag{3.27}$$

where $(p_1, u_1)$ satisfies

$$\begin{cases} u_1 - u_l = -\sqrt{(p_1 - p_l)\left(e^{-\frac{p_l}{Af(s_l)}} - e^{-\frac{p_1}{Af(s_l)}}\right)}, \\ u_r - u_1 = 2\sqrt{Af(s_r)}\left(e^{-\frac{p_1}{2Af(s_r)}} - e^{-\frac{p_r}{2Af(s_r)}}\right). \end{cases} \tag{3.28}$$

## 4. The limiting behaviors of the Riemann solutions for (1.1), (1.2), and (1.4) as $A \to 0$ with $u_l > u_r$

We now investigate the concentration phenomenon in Riemann solutions to systems (1.1), (1.2), and (1.4) for initial data belonging to Region I with $u_l > u_r$. Our objective is to elucidate the asymptotic behavior of the characteristic lines and the intermediate states as the parameter $A$ vanishes.

Fix $A > 0$. Let $(\rho_1^A, u_1^A, s_l)$ and $(\rho_2^A, u_2^A, s_r)$ denote the intermediate states satisfying the wave configuration

$$(\rho_l, u_l, s_l) \xrightarrow{S_1} (\rho_1^A, u_1^A, s_l) \xrightarrow{J_2} (\rho_2^A, u_2^A, s_r) \xrightarrow{S_3} (\rho_r, u_r, s_r). \tag{4.1}$$

Based on the elementary wave properties derived in Section III, the intermediate densities $\rho_1^A, \rho_2^A$ and the velocity $u_1^A$ are uniquely determined by the following algebraic system

$$\begin{cases} p_1^A = p_2^A, \quad u_1^A = u_2^A, \\ u_1^A - u_l = -\sqrt{(p_1^A - p_l)\left(\frac{1}{\rho_l} - \frac{1}{\rho_1^A}\right)}, \\ u_r - u_1^A = -\sqrt{(p_2^A - p_r)\left(\frac{1}{\rho_r} - \frac{1}{\rho_2^A}\right)}, \end{cases} \tag{4.2}$$

where the intermediate pressures are given by $p_1^A = Af(s_l)\ln\rho_1^A$ and $p_2^A = Af(s_r)\ln\rho_2^A$.

Furthermore, we denote the propagation speeds of $S_1$, $J_2$, and $S_3$ by $\sigma_1^A$, $\sigma_2^A$, and $\sigma_3^A$, respectively. The limiting process leading to the formation of $\delta$-shock waves is established through the following series of lemmas.

**Lemma 4.1.** *Assume that the initial data satisfies $u_l > u_r$. For any fixed pressure parameter $A > 0$, let $(\rho_1^A, u_1^A, s_l)$ and $(\rho_2^A, u_2^A, s_r)$ be the intermediate states determined by the wave configuration in Region I. Then, we have*

$$\lim_{A\to 0}\rho_1^A = +\infty, \quad \lim_{A\to 0}\rho_2^A = +\infty. \tag{4.3}$$

*Proof.* Summing the second and third equations of (4.2) yields

$$u_l - u_r = \sqrt{Af(s_l)(\ln \rho_1^A - \ln \rho_l)\left(\frac{1}{\rho_l} - \frac{1}{\rho_1^A}\right)} + \sqrt{Af(s_r)(\ln \rho_2^A - \ln \rho_r)\left(\frac{1}{\rho_r} - \frac{1}{\rho_2^A}\right)}. \tag{4.4}$$

Since $u_l - u_r > 0$ is fixed, taking $A \to 0$ forces the logarithmic terms to diverge. Thus,

$$\lim_{A\to 0} \rho_1^A = +\infty. \tag{4.5}$$

Given the pressure continuity condition $p_1^A = p_2^A$ then implies $\lim_{A\to 0} \rho_2^A = +\infty$. □

**Lemma 4.2.** *Under the same assumptions as Lemma 4.1, the intermediate pressures satisfy*

$$\lim_{A\to 0} p_1^A = \lim_{A\to 0} p_2^A = \frac{\rho_l \rho_r (u_l - u_r)^2}{(\sqrt{\rho_l} + \sqrt{\rho_r})^2}. \tag{4.6}$$

*Proof.* From (4.2), we have that

$$\begin{cases} u_1^A - u_l = -\sqrt{(p_1^A - p_l)\left(\frac{1}{\rho_l} - \frac{1}{\rho_1^A}\right)}, \\ u_r - u_1^A = -\sqrt{(p_2^A - p_r)\left(\frac{1}{\rho_r} - \frac{1}{\rho_2^A}\right)}. \end{cases} \tag{4.7}$$

Eliminating $u_1^A$ yields

$$u_l - u_r = \sqrt{(p_1^A - p_l)\left(\frac{1}{\rho_l} - \frac{1}{\rho_1^A}\right)} + \sqrt{(p_2^A - p_r)\left(\frac{1}{\rho_r} - \frac{1}{\rho_2^A}\right)}. \tag{4.8}$$

Taking $A \to 0$ in (4.8), noting $1/\rho_{1,2}^A \to 0$ and $p_{l,r} \to 0$, yields

$$u_l - u_r = \left(\frac{1}{\sqrt{\rho_l}} + \frac{1}{\sqrt{\rho_r}}\right) \lim_{A\to 0} \sqrt{p_1^A}. \tag{4.9}$$

Solving for $\lim_{A\to 0} p_1^A$ completes the proof. □

**Lemma 4.3.** *Under the same assumptions as Lemma 4.1, denote the wave speeds of $S_1$, $J_2$, and $S_3$ as $\sigma_1^A$, $\sigma_2^A$, and $\sigma_3^A$, respectively. Then, we have that*

$$\lim_{A\to 0} u_1^A = \lim_{A\to 0} \sigma_i^A = \frac{\sqrt{\rho_l} u_l + \sqrt{\rho_r} u_r}{\sqrt{\rho_l} + \sqrt{\rho_r}} := u_\delta, \quad i = 1, 2, 3, \tag{4.10}$$

*where $u_\delta$ exactly coincides with the propagation speed of the $\delta$-shock wave in the 2-D PGD model* (1.3).

*Proof.* From the second equation of (4.2) and Lemma 4.2, we obtain

$$\lim_{A\to 0} u_1^A = u_l - \lim_{A\to 0} \sqrt{p_1^A\left(\frac{1}{\rho_l} - \frac{1}{\rho_1^A}\right)} = u_l - \frac{\sqrt{\rho_r}(u_l - u_r)}{\sqrt{\rho_l} + \sqrt{\rho_r}} = \frac{\sqrt{\rho_l}u_l + \sqrt{\rho_r}u_r}{\sqrt{\rho_l} + \sqrt{\rho_r}}. \tag{4.11}$$

According to the shock speed relation and $\lim_{A\to 0}\rho_1^A = +\infty$, we also have

$$\lim_{A\to 0}\sigma_1^A = \lim_{A\to 0}\left(u_1^A - \frac{\rho_l(u_1^A - u_l)}{\rho_1^A}\right) = \frac{\sqrt{\rho_l}u_l + \sqrt{\rho_r}u_r}{\sqrt{\rho_l} + \sqrt{\rho_r}}. \tag{4.12}$$

Similarly, we deduce that $\lim_{A\to 0}\sigma_2^A = \lim_{A\to 0}\sigma_3^A = u_\delta$. This completes the proof of the lemma. □

**Lemma 4.4.** *Under the same assumptions as Lemma 4.1, the integrals of the conserved quantities over the intermediate wave regions satisfy*

$$\begin{aligned}
\lim_{A\to 0}\int_{\sigma_1^A}^{\sigma_3^A} \rho^A\,d\xi &= \sigma[\rho] - [\rho u],\\
\lim_{A\to 0}\int_{\sigma_1^A}^{\sigma_3^A} \rho^A u^A\,d\xi &= \sigma[\rho u] - [\rho u^2],\\
\lim_{A\to 0}\int_{\sigma_1^A}^{\sigma_3^A} \rho^A s^A\,d\xi &= \sigma[\rho s] - [\rho u s].
\end{aligned} \tag{4.13}$$

*Proof.* The first two limits in (4.13) are standard. For the entropy integral, applying Lemmas 4.1–4.2 alongside the Rankine-Hugoniot conditions yields

$$\begin{aligned}
\lim_{A\to 0}\int_{\sigma_1^A}^{\sigma_3^A}(\rho s)\,d\xi &= \lim_{A\to 0}\Big(\rho_2^A s_r(\sigma_3^A - \sigma_2^A) + \rho_1^A s_l(\sigma_2^A - \sigma_1^A)\Big)\\
&= \lim_{A\to 0}\left(\rho_2^A s_r\left(\frac{\rho_r u_r - \rho_2^A u_1^A}{\rho_r - \rho_2^A} - u_1^A\right) + \rho_1^A s_l\left(u_1^A - \frac{\rho_1^A u_1^A - \rho_l u_l}{\rho_1^A - \rho_l}\right)\right)\\
&= \lim_{A\to 0}\left(s_r\frac{\rho_2^A\rho_r(u_r - u_1^A)}{\rho_r - \rho_2^A} + s_l\frac{\rho_1^A\rho_l(u_l - u_1^A)}{\rho_1^A - \rho_l}\right)\\
&= \lim_{A\to 0}\Big(-\rho_r s_r(u_r - u_1^A) + \rho_l s_l(u_l - u_1^A)\Big)\\
&= \sigma[\rho s] - [\rho u s].
\end{aligned} \tag{4.14}$$

This concludes the proof. □

Lemmas 4.1–4.4 reveal that as $A \to 0$, the characteristic curves $S_1$, $J_2$, and $S_3$ coalesce, accompanied by the divergence of intermediate densities. The following theorem rigorously characterizes the associated concentration of mass, momentum, and entropy.

**Theorem 4.5.** *For $u_l > u_r$ and any fixed $A > 0$, let $(\rho^A, u^A, s^A)$ be a solution to systems* (1.1), (1.2), *and* (1.4). *Then, as $A \to 0$, the conserved quantities $\rho^A$, $\rho^A u^A$, and $\rho^A s^A$ converge in the distributional sense.*

*The limit functions $\rho, \rho u, \rho s$ consist of a step function superposed with a Dirac measure, characterized by the weights*

$$w_1(t) = t(u_\delta[\rho] - [\rho u]), \quad w_2(t) = t(u_\delta[\rho u] - [\rho u^2]), \quad w_3(t) = t(u_\delta[\rho s] - [\rho u s]), \tag{4.15}$$

*respectively.*

*Proof.* (1) For a fixed $A > 0$, the explicit Riemann solution reads

$$(\rho^A, u^A, s^A)(\xi) = \begin{cases} (\rho_l, u_l, s_l), & \xi < \sigma_1^A, \\ (\rho_1^A, u_1^A, s_l), & \sigma_1^A < \xi < \sigma_2^A, \\ (\rho_2^A, u_1^A, s_r), & \sigma_2^A < \xi < \sigma_3^A, \\ (\rho_r, u_r, s_r), & \xi > \sigma_3^A, \end{cases} \tag{4.16}$$

where $\xi = x/t$. For any test function $\varphi(\xi) \in C_0^\infty(\mathbb{R})$, the weak solutions satisfy the identities

$$\int_{-\infty}^{+\infty} \rho^A \varphi \, d\xi - \int_{-\infty}^{+\infty} \rho^A (u^A - \xi)\varphi' \, d\xi = 0, \tag{4.17a}$$

$$\int_{-\infty}^{+\infty} \rho^A u^A \varphi \, d\xi - \int_{-\infty}^{+\infty} (\rho^A u^A (u^A - \xi) + p^A)\varphi' \, d\xi = 0, \tag{4.17b}$$

$$\int_{-\infty}^{+\infty} \rho^A s^A \varphi \, d\xi - \int_{-\infty}^{+\infty} \rho^A s^A (u^A - \xi)\varphi' \, d\xi = 0. \tag{4.17c}$$

(2) We now proceed to derive the distributional limits of $\rho^A$, $\rho^A u^A$, and $\rho^A s^A$ based on (4.17).

(2a) Consider (4.17a). Split the derivative integral into four regions

$$\mathcal{I}_{mass} = \left( \int_{-\infty}^{\sigma_1^A} + \int_{\sigma_1^A}^{\sigma_2^A} + \int_{\sigma_2^A}^{\sigma_3^A} + \int_{\sigma_3^A}^{+\infty} \right) \rho^A (u^A - \xi)\varphi' \, d\xi. \tag{4.18}$$

For the outer regions, as $A \to 0$,

$$\lim_{A\to 0} \left( \int_{-\infty}^{\sigma_1^A} + \int_{\sigma_3^A}^{+\infty} \right) \rho^A (u^A - \xi)\varphi' \, d\xi = (u_\delta[\rho] - [\rho u])\varphi(u_\delta) + \int_{-\infty}^{+\infty} \rho_0 \varphi \, d\xi, \tag{4.19}$$

where $[\rho] = \rho_r - \rho_l$ and $\rho_0$ satisfies the initial condition (2.9). For the first intermediate layer $[\sigma_1^A, \sigma_2^A]$, we have

$$\begin{aligned}
&\lim_{A\to 0} \int_{\sigma_1^A}^{\sigma_2^A} \rho^A (u^A - \xi)\varphi' \, d\xi = \lim_{A\to 0} \int_{\sigma_1^A}^{\sigma_2^A} \rho_1^A (u_1^A - \xi)\varphi' \, d\xi \\
&= \lim_{A\to 0} \left\{ \rho_1^A u_1^A (\varphi(\sigma_2^A) - \varphi(\sigma_1^A)) - \rho_1^A (\sigma_2^A \varphi(\sigma_2^A) - \sigma_1^A \varphi(\sigma_1^A)) + \rho_1^A \int_{\sigma_1^A}^{\sigma_2^A} \varphi(\xi) \, d\xi \right\} \\
&= \lim_{A\to 0} \left\{ \rho_1^A (\sigma_2^A - \sigma_1^A) \left( u_1^A \frac{\varphi(\sigma_2^A) - \varphi(\sigma_1^A)}{\sigma_2^A - \sigma_1^A} - \frac{\sigma_2^A \varphi(\sigma_2^A) - \sigma_1^A \varphi(\sigma_1^A)}{\sigma_2^A - \sigma_1^A} + \frac{\int_{\sigma_1^A}^{\sigma_2^A} \varphi(\xi) \, d\xi}{\sigma_2^A - \sigma_1^A} \right) \right\} \\
&= -\rho_l (u_\delta - u_l)(u_\delta \varphi'(u_\delta) - (u_\delta \varphi(u_\delta))' + \varphi(u_\delta)) \\
&= 0.
\end{aligned} \tag{4.20}$$

Similarly, the integral over the second intermediate layer also vanishes

$$\lim_{A\to 0}\int_{\sigma_2^A}^{\sigma_3^A}\rho^A(u^A-\xi)\varphi'\,d\xi=0. \tag{4.21}$$

Consequently, summing the contributions, we get that

$$\lim_{A\to 0}\int_{-\infty}^{+\infty}(\rho^A-\rho_0)\varphi\,d\xi=(u_\delta[\rho]-[\rho u])\varphi(u_\delta). \tag{4.22}$$

(2b) For (4.17b), the same decomposition gives

$$\lim_{A\to 0}\int_{-\infty}^{+\infty}\rho^A u^A(u^A-\xi)\varphi'\,d\xi=(u_\delta[\rho u]-[\rho u^2])\varphi(u_\delta)+\int_{-\infty}^{+\infty}\rho_0u_0\varphi\,d\xi. \tag{4.23}$$

For the pressure term, using Lemmas 4.2 and 4.3, we obtain

$$\begin{aligned}\lim_{A\to 0}\int_{-\infty}^{+\infty}p^A\varphi'\,d\xi&=\lim_{A\to 0}\left(\int_{-\infty}^{\sigma_1^A}+\int_{\sigma_1^A}^{\sigma_2^A}+\int_{\sigma_2^A}^{\sigma_3^A}+\int_{\sigma_3^A}^{+\infty}\right)p^A\varphi'\,d\xi\\&=\lim_{A\to 0}\{p_l\varphi(\sigma_1^A)+p_1^A(\varphi(\sigma_2^A)-\varphi(\sigma_1^A))+p_2^A(\varphi(\sigma_3^A)-\varphi(\sigma_2^A))-p_r\varphi(\sigma_3^A)\}\\&=0.\end{aligned} \tag{4.24}$$

Substituting (4.23) and (4.24) into (4.17b) leads to

$$\lim_{A\to 0}\int_{-\infty}^{+\infty}(\rho^A u^A-\rho_0u_0)\varphi\,d\xi=(u_\delta[\rho u]-[\rho u^2])\varphi(u_\delta). \tag{4.25}$$

(2c) For (4.17c), we decompose similarly

$$\int_{-\infty}^{+\infty}\rho^A s^A(u^A-\xi)\varphi'\,d\xi=\left(\int_{-\infty}^{\sigma_1^A}+\int_{\sigma_1^A}^{\sigma_2^A}+\int_{\sigma_2^A}^{\sigma_3^A}+\int_{\sigma_3^A}^{+\infty}\right)(\rho^A s^A(u^A-\xi)\varphi')\,d\xi. \tag{4.26}$$

For the first and fourth terms of (4.26),

$$\lim_{A\to 0}\left(\int_{-\infty}^{\sigma_1^A}+\int_{\sigma_3^A}^{+\infty}\right)\rho^A s^A(u^A-\xi)\varphi'\,d\xi=(u_\delta[\rho s]-[\rho us])\varphi(u_\delta)+\int_{-\infty}^{+\infty}\rho_0s_0\varphi\,d\xi. \tag{4.27}$$

Meanwhile, the intermediate terms vanishes

$$\begin{aligned}&\lim_{A\to 0}\left(\int_{\sigma_1^A}^{\sigma_2^A}+\int_{\sigma_2^A}^{\sigma_3^A}\right)\rho^A s^A(u^A-\xi)\varphi'\,d\xi\\&=\lim_{A\to 0}\int_{\sigma_1^A}^{\sigma_2^A}\rho_1^A s_l(u_1^A-\xi)\varphi'\,d\xi+\lim_{A\to 0}\int_{\sigma_2^A}^{\sigma_3^A}\rho_2^A s_r(u_1^A-\xi)\varphi'\,d\xi\\&=0.\end{aligned} \tag{4.28}$$

Thus, combining (4.26) - (4.28), we arrive at

$$\lim_{A\to 0}\int_{-\infty}^{+\infty}(\rho^A s^A-\rho_0s_0)\varphi\,d\xi=(u_\delta[\rho s]-[\rho us])\varphi(u_\delta). \tag{4.29}$$

(3) Finally, we establish the distributional limits by incorporating the time dependence of the Dirac measure weights as $A \to 0$. For any $\psi(x,t) \in C_0^\infty(\mathbb{R} \times \mathbb{R}^+)$, we have

$$\begin{aligned}
&\lim_{A\to 0}\int_0^{+\infty}\int_{-\infty}^{+\infty}\rho^A(x,t)\psi(x,t)\,dxdt\\
&=\lim_{A\to 0}\int_0^{+\infty}\int_{-\infty}^{+\infty}\rho^A(\xi)\psi(\xi t,t)t\,d\xi dt\\
&=\int_0^{+\infty}\left(t(u_\delta[\rho]-[\rho u])\psi(u_\delta t,t)+\int_{-\infty}^{+\infty}\rho_0\psi(\xi t,t)t\,d\xi\right)dt\\
&=\langle\rho_0,\psi\rangle+\langle w_1(t)\delta_S,\psi\rangle,
\end{aligned}\tag{4.30}$$

where we find that

$$w_1(t) = t(u_\delta[\rho] - [\rho u]). \tag{4.31}$$

Similarly, we conclude

$$\lim_{A\to 0}\int_0^{+\infty}\int_{-\infty}^{+\infty}\rho^A u^A\psi\,dxdt=\int_0^{+\infty}\int_{-\infty}^{+\infty}\rho_0u_0\psi\,dxdt+\langle w_2(t)\delta_S,\psi\rangle, \tag{4.32}$$

and

$$\lim_{A\to 0}\int_0^{+\infty}\int_{-\infty}^{+\infty}\rho^A s^A\psi\,dxdt=\int_0^{+\infty}\int_{-\infty}^{+\infty}\rho_0s_0\psi\,dxdt+\langle w_3(t)\delta_S,\psi\rangle. \tag{4.33}$$

with

$$w_2(t) = t(u_\delta[\rho u] - [\rho u^2]),\quad w_3(t) = t(u_\delta[\rho s] - [\rho us]). \tag{4.34}$$

This concludes the proof. □

*Physical Interpretation.* Although the weak formulation of the $\delta$-shock established in Theorem 4.5 shares a similar mathematical structure with classical gas models, the physical mechanism driving the density concentration is fundamentally distinct. In highly compressible flows, such as astrophysical collisions or hypervelocity impacts, the kinetic energy of the incoming fluid is typically converted into internal energy and entropy. For polytropic gases, this process is effectively resisted by the algebraic growth of the pressure [19]. In contrast, the logarithmic EoS provides a relatively weak pressure response at high densities. Consequently, the fluid cannot generate strong enough pressure gradients to decelerate the incoming momentum. This leads to an extreme exponential mass concentration ($\rho \sim e^{C/A}$), causing the interfacial layer to collapse into a macroscopic singularity. This unique mechanism will be quantitatively analyzed and compared in Section 6.1.

## 5. The limiting behaviors of the Riemann solutions for (1.1), (1.2), and (1.4) with $u_l < u_r$

In this section, we discuss the cavitation phenomenon of the Riemann solutions for (1.1), (1.2), and (1.4) with $u_l < u_r$ as $A \to 0$.

**Lemma 5.1.** *For $u_l < u_r$, let $(\rho_1^A, \rho_2^A)$ and $u_1^A$ be the densities and velocity of the intermediate states. Then, in the limit $A \to 0$, both intermediate densities vanish*

$$\lim_{A\to 0}\rho_1^A = \lim_{A\to 0}\rho_2^A = 0. \tag{5.1}$$

*Moreover, the limit of the intermediate velocity* $u_{vac} := \lim_{A\to 0} u_1^A$ *is uniquely determined by the entropy ratio* $k = \frac{f(s_l)}{f(s_r)}$

$$u_{vac} = \begin{cases} u_l, & \text{if } f(s_l) > f(s_r), \\ \frac{u_l+u_r}{2}, & \text{if } f(s_l) = f(s_r), \\ u_r, & \text{if } f(s_l) < f(s_r). \end{cases} \tag{5.2}$$

*Proof.* From (3.5), (3.7), and (3.6), the Riemann solution exhibits the structure $(\rho_l, u_l, s_l) \xrightarrow{R_1} (\rho_1^A, u_1^A, s_l) \xrightarrow{J_2} (\rho_2^A, u_1^A, s_r) \xrightarrow{R_3} (\rho_r, u_r, s_r)$ if and only if the intermediate states satisfy

$$\begin{cases} u_1^A - u_l = 2\sqrt{Af(s_l)}\left((\rho_1^A)^{-\frac{1}{2}} - \rho_l^{-\frac{1}{2}}\right), \\ f(s_l)\ln\rho_1^A = f(s_r)\ln\rho_2^A, \quad \rho_1^A < \rho_l,\ \rho_2^A < \rho_r, \\ u_r - u_1^A = 2\sqrt{Af(s_r)}\left((\rho_2^A)^{-\frac{1}{2}} - \rho_r^{-\frac{1}{2}}\right). \end{cases} \tag{5.3}$$

Summing the first and third equations of (5.3) yields

$$2\sqrt{A}\left(\sqrt{\frac{f(s_l)}{\rho_1^A}} + \sqrt{\frac{f(s_r)}{\rho_2^A}}\right) = (u_r - u_l) + 2\sqrt{A}\left(\sqrt{\frac{f(s_l)}{\rho_l}} + \sqrt{\frac{f(s_r)}{\rho_r}}\right). \tag{5.4}$$

As $A \to 0$, the right-hand side tends to the positive constant $u_r - u_l$. Therefore, the left-hand side cannot vanish, which forces $\rho_1^A, \rho_2^A \to 0$. Hence, $\lim_{A\to 0}\rho_1^A = \lim_{A\to 0}\rho_2^A = 0$.

Next, to find the limit of $u_1^A$, divide the first equation by the third and take $A \to 0$. Then, we obtain

$$\frac{u_1^A - u_l}{u_r - u_1^A} \approx \frac{2\sqrt{Af(s_l)}(\rho_1^A)^{-1/2}}{2\sqrt{Af(s_r)}(\rho_2^A)^{-1/2}} = \sqrt{\frac{f(s_l)}{f(s_r)}}\left(\frac{\rho_2^A}{\rho_1^A}\right)^{1/2}. \tag{5.5}$$

From the second equation of (5.3), we have $\rho_2^A = (\rho_1^A)^{f(s_l)/f(s_r)}$. Substituting this into (5.5), we arrive at

$$\lim_{A\to 0}\frac{u_1^A - u_l}{u_r - u_1^A} = \sqrt{\frac{f(s_l)}{f(s_r)}}\lim_{A\to 0}(\rho_1^A)^{\frac{1}{2}\left(\frac{f(s_l)}{f(s_r)}-1\right)}. \tag{5.6}$$

Since $\rho_1^A \to 0$, the limit depends on the sign of the exponent. We summarize as follows

$$u_{vac} = \lim_{A\to 0} u_1^A = \begin{cases} u_l, & \text{if } f(s_l) > f(s_r), \\ \frac{u_l+u_r}{2}, & \text{if } f(s_l) = f(s_r), \\ u_r, & \text{if } f(s_l) < f(s_r). \end{cases} \tag{5.7}$$

This completes the proof. □

We now analyze the evolution of the boundaries of rarefaction waves in the $x - t$ plane as $A \to 0$.

**Lemma 5.2.** *Assume that the initial data satisfies $u_l < u_r$. For any fixed $A > 0$, as the intermediate states tend to vacuum, the characteristic speeds satisfy*

$$\begin{aligned}
&\lim_{A\to 0}\lambda_1(\rho_l,u_l,s_l)=u_l,\quad \lim_{A\to 0}\lambda_3(\rho_r,u_r,s_r)=u_r,\\
&\lim_{A\to 0}\lambda_1(\rho_1^A,u_1^A,s_l)=\frac{u_{vac}+u_l}{2}:=\lambda_1^0,\\
&\lim_{A\to 0}\lambda_3(\rho_2^A,u_1^A,s_r)=\frac{u_{vac}+u_r}{2}:=\lambda_3^0.
\end{aligned}\tag{5.8}$$

*where $u_{vac}$ is the limit velocity derived in Lemma 5.1.*

*Proof.* Since $\lambda_1 = u - \sqrt{Af(s)/\rho}$ and $\lambda_3 = u + \sqrt{Af(s)/\rho}$, we obtain that

$$\lim_{A\to 0}\lambda_1(\rho_l,u_l,s_l)=u_l,\quad \lim_{A\to 0}\lambda_3(\rho_r,u_r,s_r)=u_r.\tag{5.9}$$

From the first equation of (5.3), we have

$$\lim_{A\to 0}\sqrt{\frac{Af(s_l)}{\rho_1^A}}=\lim_{A\to 0}\frac{u_1^A-u_l}{2}.\tag{5.10}$$

Then we obtain that

$$\begin{aligned}
\lim_{A\to 0}\lambda_1(\rho_1^A,u_1^A,s_l)&=\lim_{A\to 0}\left(u_1^A-\sqrt{\frac{Af(s_l)}{\rho_1^A}}\right)=\lim_{A\to 0}\left(u_1^A-\frac{u_1^A-u_l}{2}\right)\\
&=\frac{u_{vac}+u_l}{2}:=\lambda_1^0.
\end{aligned}\tag{5.11}$$

Similarly, from the third equation of (5.3), we have

$$\lim_{A\to 0}\sqrt{\frac{Af(s_r)}{\rho_2^A}}=\lim_{A\to 0}\frac{u_r-u_1^A}{2}.\tag{5.12}$$

Thus, we get

$$\begin{aligned}
\lim_{A\to 0}\lambda_3(\rho_2^A,u_1^A,s_r)&=\lim_{A\to 0}\left(u_1^A+\sqrt{\frac{Af(s_r)}{\rho_2^A}}\right)=\lim_{A\to 0}\left(u_1^A+\frac{u_r-u_1^A}{2}\right)\\
&=\frac{u_{vac}+u_r}{2}:=\lambda_3^0.
\end{aligned}\tag{5.13}$$

Besides, we obtain the ordering of the characteristic speeds:

$$u_l\le\lambda_1^0\le u_{vac}\le\lambda_3^0\le u_r.\tag{5.14}$$

Thus, the proof is complete. □

Then, let $U_m^A = (\rho_m^A, u_m^A, s_l)$ be an intermediate state between $U_l$ and $U_1^A$, which implies

$$\begin{cases}
u_m^A-u_l=2\sqrt{Af(s_l)}\left((\rho_m^A)^{-\frac{1}{2}}-\rho_l^{-\frac{1}{2}}\right),\\
u_l<u_m^A<u_1^A.
\end{cases}\tag{5.15}$$

Taking limits on both sides of the first equation of (5.15), we obtain

$$\lim_{A\to 0}(u_m^A - u_l) = \lim_{A\to 0} 2\sqrt{Af(s_l)}(\rho_m^A)^{-\frac{1}{2}}, \tag{5.16}$$

which implies $\lim_{A\to 0}\rho_m^A = 0$.

For the intermediate state $U_n^A = (\rho_n^A, u_n^A, s_r)$ within the 3-rarefaction wave region, we obtain the similar conclusion that $\lim_{A\to 0}\rho_n^A = 0$.

Based on the preceding analysis, as $A \to 0$, the left and right boundaries of the first-family rarefaction wave rotate clockwise to the characteristic slopes corresponding to $u_l$ and $\lambda_1^0$, respectively. Simultaneously, the third-family rarefaction wave exhibits a counterclockwise rotation, with its left and right boundaries moving to the slopes defined by the velocities $\lambda_3^0$ and $u_r$, respectively. The blue dashed lines in Figure 2 represent the limiting positions of these rarefaction wave boundaries.

Crucially, the second-family contact discontinuity $J_2$, which originally separates the two intermediate states, converges to the limiting ray $x = u_{vac}t$ (indicated by the red solid lines). Its limiting position is strictly determined by the entropy ratio $f(s_l)/f(s_r)$. As illustrated in the bottom panels of Figure 2, this leads to three distinct geometric structures: when $f(s_l) > f(s_r)$, $J_2$ merges with the left contact discontinuity $J_1$ with speed $u_{vac} = u_l$; when $f(s_l) = f(s_r)$, $J_2$ stabilizes in the middle with speed $u_{vac} = \frac{u_l+u_r}{2}$; and when $f(s_l) < f(s_r)$, $J_2$ merges with the right contact discontinuity $J_3$ with speed $u_{vac} = u_r$.

Consequently, this geometric configuration drives the two intermediate non-vacuum states toward vacuum conditions. Specifically, the density within the rarefaction wave regions asymptotically approaches zero, fully realizing a vacuum state throughout the entire interval $(u_l t, u_r t)$.

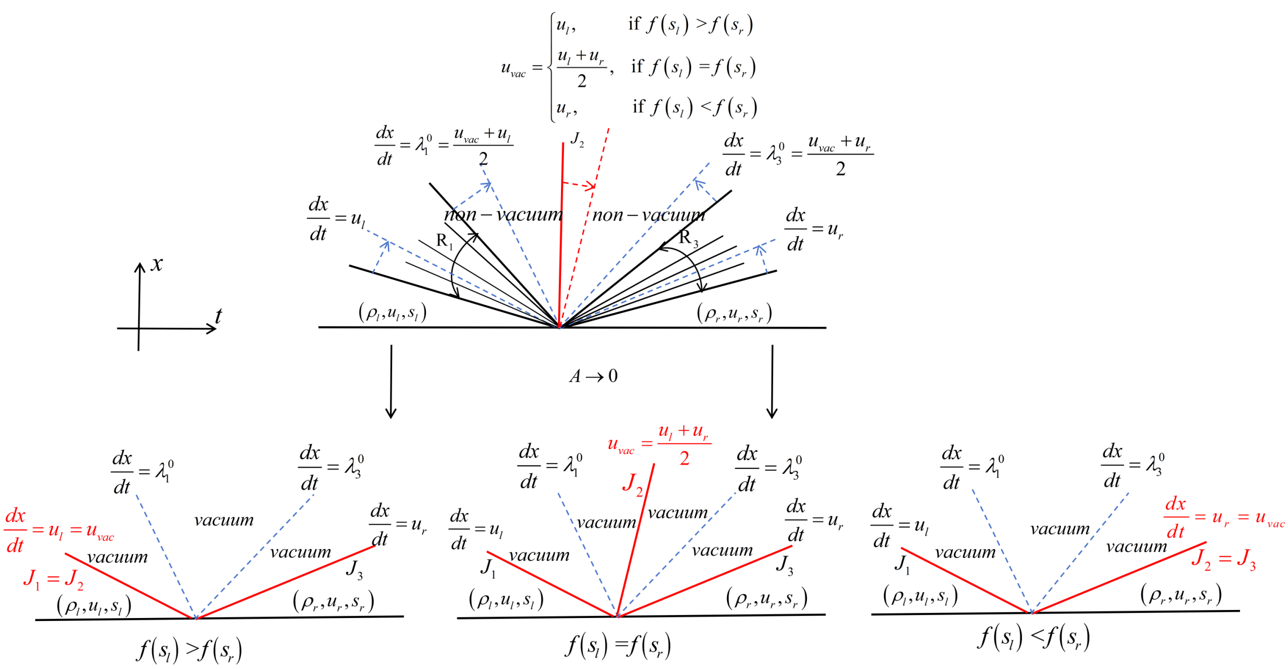


**Figure 2.** The formation mechanics of vacuum.

**Theorem 5.3.** *For systems* (1.1)*,* (1.2)*, and* (1.4) *with $u_l < u_r$, the limit of the Riemann solutions is*

$$(\rho_l, u_l, s_l) \xrightarrow{J_1} (0, x/t, s(x/t)) \xrightarrow{J_3} (\rho_r, u_r, s_r), \tag{5.17}$$

*which is the vacuum solution for the pressureless gas dynamics* (1.3) *and* (1.4)*, where $J_1$ and $J_3$ denote the contact discontinuities with speed $u_l$ and $u_r$, respectively.*

*Remark.* Unlike the simple geometric separation of wave boundaries in classical vanishing pressure limits [19,20], the vacuum generation here is driven by an intense, continuous rarefaction dilution [39]. As pressure vanishes, the logarithmic gas asymptotically evacuates the intermediate mass due to its unbounded expansibility.

Furthermore, this macroscopic evacuation exhibits a highly asymmetric thermodynamic expansion, fundamentally differing from the symmetric cavitation in isentropic cases [21]. As shown in Lemma 5.1, the spatial distribution of the vacuum is strictly determined by the entropy ratio $f(s_l)/f(s_r)$. Physically, the high-entropy phase possesses greater thermodynamic stiffness [40, 41]. During rapid expansion, it exerts a dominant pressure that suppresses the low-entropy phase, forcing the intermediate states to merge and thereby driving the macroscopic vacuum boundary entirely into the weaker fluid's domain.

## 6. Asymptotic comparisons and scaling transitions

In this section, we elucidate the fundamental differences between the non-isentropic generalized logarithmic gas and classical gas models by comparing their asymptotic behaviors as the pressure parameter $A \to 0$. Specifically, we analyze the concentration rate against the polytropic gas ($p = Af(s)\rho^{\gamma_1(A)}$) and the cavitation rate against the generalized Chaplygin gas ($p = -Af(s)\rho^{-\gamma_2(A)}$). This comparative analysis highlights the novel singular mechanisms intrinsically driven by the logarithmic nonlinearity.

### *6.1. Concentration limit: Logarithmic versus polytropic gases*

As demonstrated in Theorem 4.5, for $u_l > u_r$, the intermediate density of the generalized logarithmic gas accumulates exponentially ($\rho \sim e^{C/A}$). To appreciate the singularity of this concentration mechanism, we compare it with the classical polytropic gas governed by the equation of state $p = Af(s)\rho^{\gamma_1(A)}$ ($\gamma_1(A) > 0$). The fundamental disparity and the required scaling transition to bridge these two models are established in the following lemma.

**Lemma 6.1.** *For the Riemann problem with $u_l > u_r$, as the pressure parameter $A \to 0$, if the equivalent polytropic index $\gamma_1(A)$ satisfies the principal asymptotic condition*

$$\gamma_1(A) \sim \frac{A}{C} \ln\left(\frac{C}{A}\right), \tag{6.1}$$

*where $C = P^*/f(s_l)$ is a positive constant, then the intermediate densities of the two gas models tend to infinity at the same asymptotic rate, achieving the exact exponential concentration $O(e^{C/A})$.*

*Proof.* Applying the analogous generalized Rankine-Hugoniot conditions as $A \to 0$, the intermediate pressure $p_1^A$ for the polytropic gas converges to the same strictly positive constant $P^*$ as derived in

Lemma 4.2

$$P^* = \lim_{A\to 0} p_1^A = \frac{\rho_l \rho_r (u_l - u_r)^2}{(\sqrt{\rho_l} + \sqrt{\rho_r})^2}. \tag{6.2}$$

Let $C = P^*/f(s_l)$. For the generalized logarithmic gas, the intermediate density asymptotically behaves as $\rho_{\log}^A \sim \exp(C/A)$. Substituting the polytropic equation of state $p_1^A = Af(s_l)(\rho_{\text{poly}}^A)^{\gamma_1(A)}$, the intermediate density for the polytropic gas is

$$\rho_{\text{poly}}^A = \left(\frac{p_1^A}{Af(s_l)}\right)^{\frac{1}{\gamma_1(A)}} \sim \left(\frac{C}{A}\right)^{\frac{1}{\gamma_1(A)}}. \tag{6.3}$$

To match the asymptotic rates, we require that

$$\lim_{A\to 0} \frac{\rho_{\log}^A}{\rho_{\text{poly}}^A} = \lim_{A\to 0} \frac{\exp(C/A)}{(C/A)^{1/\gamma_1(A)}} = K > 0. \tag{6.4}$$

Taking the natural logarithm on both sides yields

$$\lim_{A\to 0} \ln\left[\frac{\exp(C/A)}{(C/A)^{1/\gamma_1(A)}}\right] = \ln K, \tag{6.5}$$

which simplifies to

$$\lim_{A\to 0}\left(\frac{C}{A} - \frac{1}{\gamma_1(A)}\ln\left(\frac{C}{A}\right)\right) = \ln K. \tag{6.6}$$

Dividing by $\ln(C/A)$ leads to

$$\lim_{A\to 0}\left(\frac{C}{A\ln(C/A)} - \frac{1}{\gamma_1(A)}\right) = 0, \tag{6.7}$$

which identifies the principal scaling of the adiabatic index as

$$\gamma_1(A) \sim \frac{A}{C}\ln\left(\frac{C}{A}\right). \tag{6.8}$$

This completes the proof. □

*6.2. Cavitation limit: Logarithmic versus generalized Chaplygin gases*

For $u_l < u_r$, we compare the cavitation rate of the logarithmic gas with the generalized Chaplygin gas ($p = -Af(s)\rho^{-\gamma_2(A)}$, $\gamma_2(A) > 0$) [35, 36]. The following lemma establishes the phase transition required to align their macroscopic decay scales.

**Lemma 6.2.** *For the Riemann problem with $u_l < u_r$, as $A \to 0$, if the equivalent index $\gamma_2(A)$ satisfies*

$$\gamma_2(A) = \begin{cases} \frac{f(s_l)}{f(s_r)} - 1, & \text{if } f(s_l) \geq f(s_r), \\ \frac{f(s_r)}{f(s_l)} - 1, & \text{if } f(s_l) < f(s_r), \end{cases} \tag{6.9}$$

*then the macroscopic cavitation scales of the generalized Chaplygin gas and the logarithmic gas decay at the exact same asymptotic rate.*

*Proof.* For the generalized Chaplygin gas, the sound speed $c = \sqrt{Af(s)\gamma_2(A)}\rho^{-\frac{\gamma_2(A)+1}{2}}$ yields the Riemann invariant integral $\int \frac{c}{\rho} d\rho = -\frac{2\sqrt{Af(s)\gamma_2(A)}}{\gamma_2(A)+1}\rho^{-\frac{\gamma_2(A)+1}{2}}$. The invariant relations across the rarefaction waves are

$$\begin{cases} u_1^A - u_l = \frac{2\sqrt{Af(s_l)\gamma_2(A)}}{\gamma_2(A)+1}\left((\rho_1^A)^{-\frac{\gamma_2(A)+1}{2}} - \rho_l^{-\frac{\gamma_2(A)+1}{2}}\right), \\ u_r - u_1^A = \frac{2\sqrt{Af(s_r)\gamma_2(A)}}{\gamma_2(A)+1}\left((\rho_2^A)^{-\frac{\gamma_2(A)+1}{2}} - \rho_r^{-\frac{\gamma_2(A)+1}{2}}\right). \end{cases} \tag{6.10}$$

Summing (6.10) and neglecting finite initial terms as $A \to 0$ yields

$$\frac{2\sqrt{\gamma_2(A)}}{\gamma_2(A)+1}\left(\sqrt{f(s_l)}(\rho_1^A)^{-\frac{\gamma_2(A)+1}{2}} + \sqrt{f(s_r)}(\rho_2^A)^{-\frac{\gamma_2(A)+1}{2}}\right) \approx \frac{u_r - u_l}{\sqrt{A}}. \tag{6.11}$$

Pressure continuity $f(s_l)(\rho_1^A)^{-\gamma_2(A)} = f(s_r)(\rho_2^A)^{-\gamma_2(A)}$ gives $\rho_2^A = \left(\frac{f(s_r)}{f(s_l)}\right)^{1/\gamma_2(A)}\rho_1^A$. Substituting into (6.11) yields

$$\rho_1^A \sim \rho_2^A \sim O\left(A^{\frac{1}{\gamma_2(A)+1}}\right). \tag{6.12}$$

For the logarithmic gas, pressure continuity $f(s_l)\ln\rho_1^A = f(s_r)\ln\rho_2^A$ gives $\rho_2^A = (\rho_1^A)^{f(s_l)/f(s_r)}$. Substituting into (5.4) yields

$$\sqrt{f(s_l)}(\rho_1^A)^{-1/2} + \sqrt{f(s_r)}(\rho_1^A)^{-\frac{f(s_l)}{2f(s_r)}} \approx \frac{u_r - u_l}{2\sqrt{A}}. \tag{6.13}$$

The macroscopic scale is governed by the slower decaying density (the less negative exponent). For $f(s_l) < f(s_r)$, the first term dominates, yielding $\rho_1^A \sim O(A)$ and $\rho_2^A \sim O\left(A^{\frac{f(s_l)}{f(s_r)}}\right)$. For $f(s_l) > f(s_r)$, the second term dominates, yielding $\rho_1^A \sim O\left(A^{\frac{f(s_r)}{f(s_l)}}\right)$. Thus, the macroscopic cavitation scale is bounded by

$$\rho_{\log}^A \sim O\left(A^{\min\left(\frac{f(s_l)}{f(s_r)}, \frac{f(s_r)}{f(s_l)}\right)}\right). \tag{6.14}$$

Aligning the asymptotic exponents from (6.12) and (6.14) gives

$$\frac{1}{\gamma_2(A)+1} = \min\left(\frac{f(s_l)}{f(s_r)}, \frac{f(s_r)}{f(s_l)}\right). \tag{6.15}$$

Solving for $\gamma_2(A)$ yields (6.9). This completes the proof. □

*Remark.* The continuous piecewise function derived in Lemma 6.2 underscores the extreme structural instability inherent to the logarithmic model. While the generalized Chaplygin gas cavitates symmetrically, the highly asymmetric thermodynamic expansion of the logarithmic gas effectively suppresses the fluid phase with lower entropic stiffness. Consequently, aligning their macroscopic vacuum boundaries necessitates a sharp phase transition in the equivalent index $\gamma_2(A)$, which mathematically preserves continuity at the threshold $f(s_l) = f(s_r)$ while perfectly reflecting the transition of the vacuum region $u_{vac}$.

## 7. Numerical simulations

In this section, we present numerical experiments to verify the formation of concentration and cavitation as the pressure parameter $A$ vanishes for the non-isentropic generalized logarithmic gas dynamics model. We employ the weighted essentially non-oscillatory (ENO) scheme for spatial discretization and a third-order Runge-Kutta method for time discretization to solve system (1.1) with the equation of state (1.2). The computational domain is set to $[0, 1]$ with $N = 3600$ grid points, and the CFL number is taken as 0.1. The numerical results at time $t = 0.2$ are presented to illustrate the limiting behaviors.

**Case 1.** Formation of $\delta$-shock waves.

To investigate the concentration phenomenon when $u_l > u_r$, we consider the following initial Riemann data

$$(\rho, u, s)|_{t=0} = \begin{cases} (0.2, 0.5, 0.25), & x < 0.5, \\ (0.1, 0.05, 0.15), & x > 0.5. \end{cases} \tag{7.1}$$

In this case, we choose the pressure perturbation parameters as $A = 1$, $A = 0.1$, and $A = 0.01$. The numerical results are displayed in Figure 3. In the figures, the blue, red, and black lines represent density $\rho$, velocity $u$, and entropy $s$, respectively.

From Figure 3, we can observe that as $A \to 0$, the density profile $\rho$ exhibits a highly localized concentration, forming a sharp spike that approximates a Dirac delta measure. Simultaneously, the velocity $u$ and entropy $s$ develop into step functions with discontinuities at the shock location. This phenomenon strictly confirms the theoretical prediction of Theorem 4.5, demonstrating that the Riemann solution converges to a $\delta$-shock wave solution of the 2-D PGD model as the pressure vanishes.

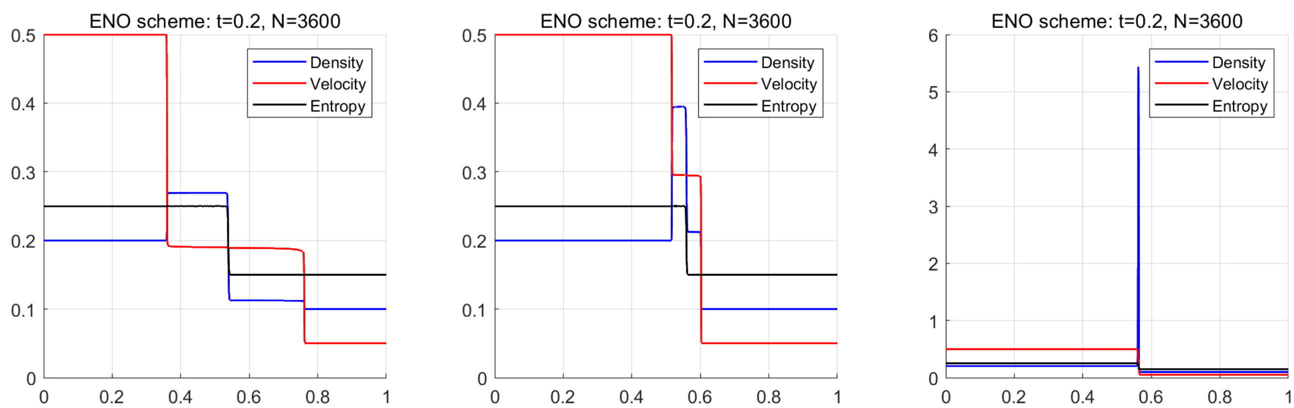


$A = 1$ $A = 0.1$ $A = 0.01$

**Figure 3.** $\rho, u, s$ for Riemann solutions of (1.1) and (7.1) with different $A$.

**Case 2.** Formation of vacuum states.

To investigate the cavitation phenomenon when $u_l < u_r$, we consider the following initial Riemann data

$$(\rho, u, s)|_{t=0} = \begin{cases} (0.2, 0.1, 0.15), & x < 0.5, \\ (0.1, 0.3, 0.25), & x > 0.5. \end{cases} \tag{7.2}$$

In this case, the simulations are performed with $A = 10^{-2}$, $A = 10^{-4}$, and $A = 10^{-6}$. The numerical results are presented in Figure 4.

As shown in Figure 4, as $A$ decreases, the density in the intermediate region rapidly decays. Specifically, when $A = 10^{-6}$, the intermediate density effectively vanishes ($\rho \approx 0$), forming a "U"-shaped vacuum region. Furthermore, the velocity profile in the vacuum region exhibits a linear distribution, which is consistent with the characteristic vacuum solution $u = x/t$ of the pressureless gas dynamics. These results rigorously verify the analytical conclusions in Theorem 5.3 regarding the formation of vacuum states.

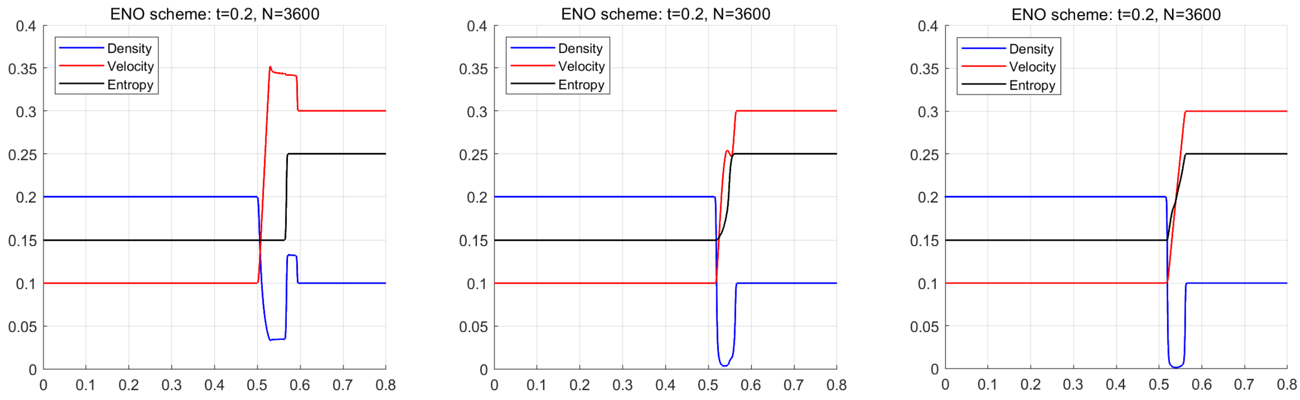


$A = 10^{-2}$ $A = 10^{-4}$ $A = 10^{-6}$

**Figure 4.** $\rho, u, s$ for Riemann solutions of (1.1) and (7.2) with different $A$.

## 8. Conclusions

In this paper, we investigated the pressureless limit of Riemann solutions for a reduced two-phase mixture model governed by a non-isentropic logarithmic equation of state. Overcoming the failure of the classical $\rho - u$ plane projection method for non-isentropic models, we constructed exact Riemann solutions directly within the $p - u - s$ phase space. As the pressure vanishes ($A \to 0$), we demonstrated two distinct singular limiting behaviors dictated by the initial velocity conditions. For $u_l > u_r$, the solutions converge to $\delta$-shock waves driven by extreme mass concentration. For $u_l < u_r$, an asymmetric vacuum emerges, where the spatial evacuation is dominated by entropy. Furthermore, through asymptotic comparisons with polytropic gases and generalized Chaplygin gases, we quantitatively demonstrated that the logarithmic gas serves as a transitional form between these two models. These analytical findings are thoroughly validated by ENO numerical simulations.

## Author contributions

Yiming Gao: Conceptualization; methodology; formal analysis; writing—original draft preparation. Weifeng Jiang: Conceptualization; methodology; formal analysis;Supervision; funding acquisition; writing—review and editing. Chengkai Tu: Validation; software; investigation. All authors have read and approved the final version of the manuscript for publication.

## Use of Generative-AI tools declaration

The authors declare they have not used Artificial Intelligence (AI) tools in the creation of this article.

## Acknowledgments

The authors would like to thank the editors and referees for providing very useful suggestions to improve the presentation in this paper. The research of Weifeng Jiang is supported by the National Natural Science Foundation of China (Grant No. 1240012056).

## Conflict of interest

The authors declare that they have no conflict of interest.

## References

1. F. Bereux, E. Bonnetier, P. G. LeFloch, Gas dynamics system: two special cases, *SIAM J. Math. Anal.,* **28** (1997), 499–515. https://doi.org/10.1137/S0036141095285831
2. T. Zhang, The invariant region for the special gas dynamics system, *Nonlinear Analysis: Real World Applications,* **38** (2017), 68–77. https://doi.org/10.1016/j.nonrwa.2017.04.007
3. Z. Bilicki, J. Kestin, Physical aspects of the relaxation model in two-phase flow, *Proceedings of the Royal Society of London. A. Mathematical and Physical Sciences,* **428** (1990), 379–397. https://doi.org/10.1098/rspa.1990.0040
4. K. Minemura, T. Uchiyama, Three-dimensional calculation of air-water two-phase flow in centrifugal pump impeller based on a bubbly flow model, 1993. https://doi.org/10.1115/1.2910210
5. L. C. ENPC, Euler system modeling vaporizing sprays, *Dynamics of Heterogeneous Combustion and Reacting Systems,* **152** (1993), 280. https://doi.org/10.2514/5.9781600866258.0280.0305
6. J.-P. Poirier, A. Tarantola, A logarithmic equation of state, *Phys. Earth Planet. Inter.,* **109** (1998), 1–8. https://doi.org/10.1016/S0031-9201(98)00112-5
7. Z. Lei, Z. Shao, Concentration and cavitation in the vanishing pressure limit of solutions to the relativistic Euler equations with the logarithmic equation of state, *J. Math. Phys.,* **64** (2023). https://doi.org/10.1063/5.0157277
8. P.-H. Chavanis, Is the Universe logotropic?, *The European Physical Journal Plus,* **130** (2015), 130. https://doi.org/10.1140/epjp/i2015-15130-5
9. S. D. Odintsov, V. K. Oikonomou, A. V. Timoshkin, E. N. Saridakis, R. Myrzakulov, Cosmological fluids with logarithmic equation of state, *Annals of Physics,* **398** (2018), 238–253. https://doi.org/10.1016/j.aop.2018.09.015
10. V. K. Oikonomou, Generalized logarithmic equation of state in classical and loop quantum cosmology dark energy-dark matter coupled systems, *Annals of Physics,* **409** (2019), 167934. https://doi.org/10.1016/j.aop.2019.167934

11. S. Li, Formation of delta-shocks for the Chaplygin gas equations by logarithmic pressure perturbation, *Rocky MT J. Math.,* **53** (2023), 1189–1209. https://doi.org/10.1216/rmj.2023.53.1189

12. E. Weinan, Y. G. Rykov, Y. G. Sinai, Generalized variational principles, global weak solutions and behavior with random initial data for systems of conservation laws arising in adhesion particle dynamics, *Commun. Math. Phys.,* **177** (1996), 349–380. https://doi.org/10.1007/BF02101897

13. Y. Brenier, E. Grenier, Sticky Particles and Scalar Conservation Laws, *SIAM J. Numer. Anal.,* **35** (1998), 2317–2328. https://doi.org/10.1137/S0036142997317353

14. S. F. Shandarin, Y. B. Zeldovich, The large-scale structure of the universe: Turbulence, intermittency, structures in a self-gravitating medium, *Rev. Mod. Phys.,* **61** (1989), 185. https://doi.org/10.1103/RevModPhys.61.185

15. K. D. Squires, J. K. Eaton, Preferential concentration of particles by turbulence, *Physics of Fluids A: Fluid Dynamics,* **3** (1991), 1169–1178. https://doi.org/10.1063/1.858045

16. D. A. Demir, Vacuum energy as the origin of the gravitational constant, *Found. Phys.,* **39** (2009), 1407–1425. https://doi.org/10.1007/s10701-009-9364-z

17. J. Hu, One-dimensional Riemann problem for equations of constant pressure fluid dynamics with measure solutions by the viscosity method, *Acta Appl. Math.,* **55** (1999), 209–229. https://doi.org/10.1023/A:1006101529302

18. J. Li, Note on the compressible Euler equations with zero temperature, *Appl. Math. Lett.,* **14** (2001), 519–523. https://doi.org/10.1016/S0893-9659(00)00187-7

19. G.-Q. Chen, H. Liu, Concentration and cavitation in the vanishing pressure limit of solutions to the Euler equations for nonisentropic fluids, *Physica D,* **189** (2004), 141–165. https://doi.org/10.1016/j.physd.2003.09.039

20. G.-Q. Chen, H. Liu, Formation of $\delta$-shocks and vacuum states in the vanishing pressure limit of solutions to the Euler equations for isentropic fluids, *SIAM J. Math. Anal.,* **34** (2003), 925–938. https://doi.org/10.1137/S0036141001399350

21. M. Sun, Concentration and cavitation phenomena of Riemann solutions for the isentropic Euler system with the logarithmic equation of state, *Nonlinear Analysis: Real World Applications,* **53** (2020), 103068. https://doi.org/10.1016/j.nonrwa.2019.103068

22. M. Sun, The intrinsic phenomena of cavitation and concentration in Riemann solutions for the isentropic two-phase model with the logarithmic equation of state, *J. Math. Phys.,* **62** (2021). https://doi.org/10.1063/5.0058618

23. X. Xin, M. Sun, The vanishing pressure limits of Riemann solutions for the Aw-Rascle hydrodynamic traffic flow model with the logarithmic equation of state, *Chaos, Solitons & Fractals,* **181** (2024), 114671. https://doi.org/10.1016/j.chaos.2024.114671

24. Y. Zhang, Q. Dai, Riemann problem and vanishing pressure limit of solutions to the isentropic relativistic Euler equations for logarithmic gas, *Phys. Fluids,* **37** (2025), 036134. https://doi.org/10.1063/5.0260629

25. S. Li, H. Wang, Riemann problems for the pressureless Euler equations modelling acoustic generation, *Revista de la Real Academia de Ciencias Exactas, Físicas y Naturales. Serie A. Matemáticas,* **119** (2025), 62. https://doi.org/10.1007/s13398-025-01731-2

26. S. Li, H. Wang, Limiting behavior of non-self-similar Riemann solutions for the Umami Chaplygin Aw-Rascle model with friction, *Phys. Fluids,* **37** (2025), 056119. https://doi.org/10.1063/5.0268058

27. W. Jiang, Y. Zhang, T. Li, T. Chen, The cavitation and concentration of Riemann solutions for the isentropic Euler equations with isothermal dusty gas, *Nonlinear Analysis: Real World Applications,* **71** (2023), 103761. https://doi.org/10.1016/j.nonrwa.2022.103761

28. Y. Zhang, J. Wu, Y. Zhang, Limits of Riemann solutions to the compressible fluid flow with logarithmic pressure, *Appl. Anal.,* **104** (2025), 1036–1062. https://doi.org/10.1080/00036811.2024.2426096

29. T. Li, Y. Fan, The vanishing pressure limits in Riemann solutions for the non-isentropic Euler equations with combined pressure and time-dependent source term, *Chaos, Solitons & Fractals,* **207** (2026), 118013. https://doi.org/10.1016/j.chaos.2026.118013

30. J. Smoller, *Shock waves and reaction-diffusion equations*, Springer Science & Business Media, 2012.

31. H. Yang, Riemann problems for a class of coupled hyperbolic systems of conservation laws, *J. Differ. Equations,* **159** (1999), 447–484. https://doi.org/10.1006/jdeq.1999.3629

32. F. Huang, Weak solution to pressureless type system, *Communications in Partial Difference Equations,* **30** (2005), 283–304. https://doi.org/10.1081/PDE-200050026

33. W. Sheng, G. Wang, G. Yin, Delta wave and vacuum state for generalized Chaplygin gas dynamics system as pressure vanishes, *Nonlinear Analysis: Real World Applications,* **22** (2015), 115–128. https://doi.org/10.1016/j.nonrwa.2014.08.007

34. Y. Zhang, S. Fan, Y. Zhang, Concentration and cavitation in the vanishing pressure limit of solutions to a 3x3 generalized Chaplygin gas equations, *Math. Model. Nat. Pheno.,* **17** (2022), 10. https://doi.org/10.1051/mmnp/2022009

35. C. Shen, M. Sun, Z. Wei, Concentration and cavitation for the modified Chaplygin two-phase flow model at the vanishing pressure limit, *Chaos, Solitons & Fractals,* **201** (2025), 117343. https://doi.org/10.1016/j.chaos.2025.117343

36. A. Singhal, A. Bhardwaj, R. Arora, Self-similar behavior of shock waves in generalized Chaplygin gas, *Chaos, Solitons & Fractals,* **207** (2026), 118023. https://doi.org/10.1016/j.chaos.2026.118023

37. G.-S. Jiang, C.-W. Shu, Efficient implementation of weighted ENO schemes, *J. Comput. Phys.,* **126** (1996), 202–228. https://doi.org/10.1006/jcph.1996.0130

38. J. Hu, The Riemann problem for a two-dimensional hyperbolic system of conservation laws with non-classical shock waves, *Acta Math. Sci.,* **18** (1998), 45–56. https://doi.org/10.1016/S0252-9602(17)30688-4

39. P. Mora, T. Grismayer, Rarefaction acceleration and kinetic effects in thin-foil expansion into a vacuum, *Phys. Rev. Lett.,* **102** (2009), 145001. https://doi.org/10.1103/PhysRevLett.102.145001

40. R. Menikoff, B. J. Plohr, The Riemann problem for fluid flow of real materials, *Rev. Mod. Phys.*, **61** (1989), 75. https://doi.org/10.1103/RevModPhys.61.75

41. R. Courant, K. O. Friedrichs, *Supersonic flow and shock waves*, Springer Science & Business Media, 1999.

AIMS Press